Colloids and Surfaces A: Physicochemical and Engineering Aspects 680 (2024) 132675

Contents lists available at ScienceDirect

Colloids and Surfaces A: Physicochemical and Engineering Aspects

journal homepage: www.elsevier.com/locate/colsurfa

Design and synthesis of bifunctional conjugated microporous polymers containing tetraphenylethene and bisulfone units for energy storage and fluorescent sensing of p-nitrophenol

Mohamed Gamal Mohamed [a,b,*,1], Huan-Yu Hu [a,1], S. Santhoshkumar [c], Manivannan Madhu [c], Tharwat Hassan Mansoure [b], Ching-Wen Hsiao [a], Yunsheng Ye [a], Cheng-Wei Huang [d], Wei-Lung Tseng [c], Shiao-Wei Kuo [a,e,*]

[a] Department of Materials and Optoelectronic Science, College of Semiconductor and Advanced Technology Research, Center for Functional Polymers and Supramolecular Materials, National Sun 'Yat-Sen University, Kaohsiung 804, Taiwan, ROC
[b] Chemistry Department, Faculty of Science, Assiut University, Assiut 71515, Egypt
[c] Department of Chemistry, National Sun Yat-sen University, Kaohsiung 804, Taiwan, ROC
[d] Department of Chemical and Materials Engineering, National Kaohsiung University of Science and Technology, Kaohsiung 80778, Taiwan, ROC
[e] Department of Medicinal and Applied Chemistry, Kaohsiung Medical University, Kaohsiung 807, Taiwan, ROC

HIGHLIGHTS

- TPE-Ph-Th, TPE-Ph-Tha, and TPE-Ph-BSu CMPs were synthesized.
- The TPE-Ph-BSu CMP, displayed excellent T_{d10} of 535 °C and a char yield of 73 wt%.
- The TPE-Ph-Th CMP, which had S_{BET} of 67 m^2 g^{-1} and a pore size of 2.0 nm.
- Both TPE-Ph-Tha and TPE-Ph-BSu CMPs demonstrated excellent supercapacitive activity.
- The TPE-Ph-BSu CMP-based fluorophores could be used for the detection of PNP.

GRAPHICAL ABSTRACT

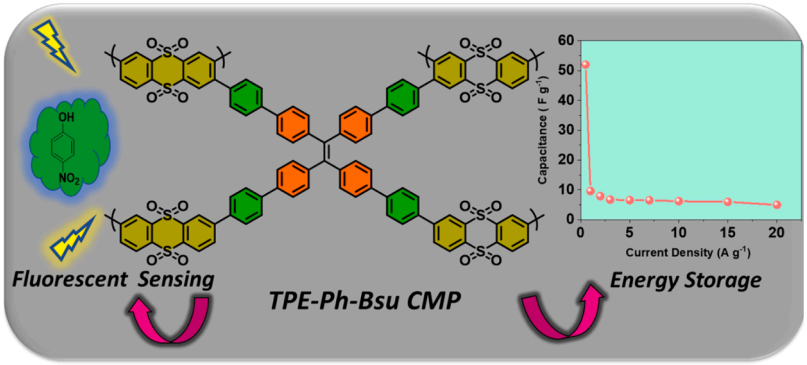

ARTICLE INFO

Keywords:
Tetraphenylethene
Suzuki coupling reaction
Conjugated microporous polymers
Supercapacitor
Chemical sensing

ABSTRACT

In this study, we successfully used the Suzuki-Miyaura reaction to prepare three novel conjugated microporous polymers (CMPs) that include tetraphenylethene (TPE): TPE-Ph-Th, TPE-Ph-Tha, and TPE-Ph-BSu. Using methods like FTIR and solid-state NMR, we examined the chemical composition and functional groups in the TPE-Ph CMPs. The TPE-Ph-BSu CMP's thermal characteristics were also examined, and they showed remarkable features with a decomposition temperature (T_{d10}) of 535 °C and a char yield of 73 wt%. We also looked at TPE-Ph-Th CMP, which had a pore size of 2.0 nm and a surface area (S_{BET}) of 67 m^2 g^{-1}. We carried out

* Corresponding authors at: Department of Materials and Optoelectronic Science, College of Semiconductor and Advanced Technology Research, Center for Functional Polymers and Supramolecular Materials, National Sun 'Yat-Sen University, Kaohsiung 804, Taiwan, ROC.
E-mail addresses: mgamal.eldin12@yahoo.com (M.G. Mohamed), kuosw@faculty.nsysu.edu.tw (S.-W. Kuo).
[1] These two authors contributed equally.

https://doi.org/10.1016/j.colsurfa.2023.132675
Received 19 August 2023; Received in revised form 18 October 2023; Accepted 27 October 2023
Available online 28 October 2023

photoluminescence (PL) and electrochemical investigations to evaluate the potential of TPE-Ph CMPs for supercapacitor applications and their capability to detect p-nitrophenol (PNP). According to our electrochemical investigation, the TPE-Ph-Tha and TPE-Ph-BSu CMPs both exhibited exceptional capacitance, reaching 51 and 52 F g^{-1} at a current density of 0.5 A g^{-1}, respectively. Furthermore, even after 5000 cycles, these CMPs still retained 80% of their capacitance, demonstrating their remarkable capacitance retention. In conclusion, synthetic TPE-Ph CMPs have several benefits, including outstanding electrochemical performance and thermal stability. Additionally, they successfully detect PNP using fluorescence-based sensing without interference, making them adaptable materials suited for a variety of applications, including the detection of pollutants (as PNP has shown) and the usage of supercapacitors.

1. Introduction

The great demand of energy to bear the economic growth nowadays directly induces climate change and environmental pollution due to the majority of energy coming out from fossil fuels. To overcome this situation, more and more research is on how to use natural power such as solar, tidal, or wind energy to replace fossil fuels [1–6]. Those natural resources have a high potential to satisfy our demand for energy. However, it has a vital problem: most of nature's power cannot produce energy 24 h a day. It may be limited by weather, time, and geographical conditions. As a result, it is critical to conceive an efficient device to store energy and solve the present situation [7,8]. Supercapacitors (SCs) are one of the most motivated electronic appliances in recent years because of their outstanding advantages at storing energy, higher power density, cycle stability, and longer cycling life, the energy density of supercapacitors is smaller than the secondary battery (Rechargeable battery) [9–11]. Furthermore, conventional dielectric capacitors and supercapacitors differ in terms of their energy storage mechanisms, energy density, charge-discharge rates, cycle stability, and the duration for which they can store energy. Supercapacitors are favored for their high-power capabilities and cycle stability, while conventional capacitors are preferred for applications requiring longer energy storage durations [9–11]. However, the main defect in SCs is the small working potential window. The electrolyte decomposes when the voltage that is provided is too high. Besides, the ability of the supercapacitor is intensely relative to the electrode materials. In the past, inorganic materials were the widest application in supercapacitors, but they greatly impacted the environment. In search of more suitable material to overcome those shortcomings, the development of polymer will play a critical role in supercapacitors [12–26]. Porous organic polymers (POPs) have been researched vigorously for decades. It presents wide applications including pollutant removal, hydrogen evolution, metal ions sensing, energy storage, CO_2 capture, photoluminescence, and the positive electrode materials in lithium-sulfur batteries, due to their high S_{BET}, variable pore diameters, chemical inertness, improved electrical conductivity and low density than inorganic materials [27–40]. If used the porous diameter of materials distinguishes the materials can be classified into three types, The International Union of Pure and Applied Chemistry (IUPAC) defines three types of porous materials: microporous materials with a diameter of less than 2 nm, mesoporous materials with a diameter of 2–50 nm, and macroporous materials with a diameter of more than 50 nm [41–46]. Another method often used for classification is crystallinity, we can divide into two sorts, one is crystalline structure such as covalent organic frameworks (COFs) [47,48] and the other is amorphous disorder structure like hyper-crosslinked polymers (HCPs) [49], covalent triazine frameworks (CTFs) [50], and CMPs. CMPs have exceptional electrochemical performance and luminous capabilities because of their pi-conjugated structure with redox activity. Furthermore, CMPs can be synthesized by a variety of methods such as oxidative polymerization, Sonogashira−Hagihara, and Yamamoto-coupling, and they lead to CMPs having a multiplicity structure and properties [51–54]. The straightforward and dependable chemical composition of TPE makes it a promising ingredient for the development of luminous materials. The McMurry coupling process offers a convenient method for producing pristine TPE and its various topological structures. TPE is an archetypal luminogen having a straightforward molecular structure and a propeller-like conformation that allows it to be recognized as a typical AIE luminophore. TPE and its derivatives both displayed poor fluorescence emission in the solution state but significant fluorescence emission in the aggregation state [55–60]. Mousa et al. presented findings on Py-PDT POP, showcasing an impressive capacitance of 28 F g^{-1} [61]. Duan group prepared CoPc-CMP with a capacitance of 13.8 F g^{-1} [62]. Mohamed et al. revealed that Py-BSU CMP had a capacitance of 38 F g^{-1} at 0.5 A g^{-1} [63]. Kuo et al. discovered that PE-Ph-Pery and TPA-Ph-Pery CMPs exhibited capacitances of 82 and 68 F g^{-1}, respectively [64]. Our group uncovered that 3D-Try-PyT CMP demonstrated its highest capacitance at 0.5 A g^{-1}, reaching a value of 66 F g^{-1} [65]. To our current understanding, we have not encountered any previous instances of TPE-based CMPs (TPE-Ph-Th, TPE-Ph-Tha, and TPE-Ph-BSu CMPs) being synthesized or employed in the context of energy storage and their application in sensing for PNP. In this investigation, utilizing the Suzuki-Miyaura reaction, we successfully synthesized three novel CMPs with the names TPE-Ph-Th, TPE-Ph-Tha, and TPE-Ph-BSu. These CMPs all include a TPE unit. We analyzed the TPE-Ph CMPs framework using methods such as FTIR and solid-state NMR in order to learn more about the chemical structure and functional groups that are present. To assess the thermal character of the TPE-Ph-BSu CMP, we also performed thermogravimetric studies (TGA). This material demonstrated good properties, having a T_{d10} of 535 °C with a char yield of up to 72 wt%. The S_{BET} and pore size of the TPE-Ph-Th CMP were both 67 m^2 g^{-1}. We conducted photoluminescence (PL) and electrochemical studies to evaluate the benefits of TPE-Ph CMPs in detecting *p*-nitrophenol and SCs applications. According to our electrochemical investigation, the TPE-Ph-Tha and TPE-Ph-BSu CMPs both displayed remarkable capacitance of 51 and 52 F g^{-1} at 0.5 A g^{-1}, respectively. Both TPE-Ph-Tha and TPE-Ph-BSu CMPs retained 80% of their capacitance for 5000 cycles, further demonstrating the extraordinary capacitance retention of these CMPs precursors. To sum up, the materials made from synthetic TPE-Ph CMPs have a number of benefits, including outstanding electrochemical performance and thermal stability. These characteristics make them intriguing materials for a variety of uses, including the detection of *p*-nitrophenol and the use of supercapacitors.

2. Experimental section

2.1. Materials

Dichloromethane (DCM), pyrene (Py), 1,4-phenylenediboronic acid (1,4-Ph-$B(OH)_2$), thianthrene (Th) bromine solution (Br_2), *p*-nitrophenol (PNP), potassium carbonate (K_2CO_3), and $Pd(PPh_3)_4$ were purchased from Sigma–Aldrich. Tetraphenylethene (TPE) and 1,3,6,8-tetrabromopyrene (Py-Br_4), were synthesized using previously reported procedures [33,37].

2.2. Synthesis of Tetrakis(4-bromophenyl)ethylene (TPE-Br_4)

DCM (94 mL), acetic acid (AcOH, 31 mL), and TPE (2.5 g, 7.53 mmol) were added into 250 mL of the two-necked round bottom flask

and soaked in salt-ice-water (0 °C) for a while. Subsequently, Br_2 (2.5 g, 31.3 mmol) was added dropwise. After returning to ambient temperature, the solution was stirred overnight. In order to obtain the product, the mixture was washed well with $Na_2S_2O_3$ and used DCM to extract before being dried with $MgSO_4$. Next, the solids were recrystallized several times with EtOH to purify and obtain a white solid (4.5 g).

2.3. Synthesis of Synthesis of 2,3,7,8-tetrabromothianthrene (Th-Br_4)

Th (3.24 g, 15 mmol), excess Br_2 (15 mL), and AcOH (60 mL) were added directly to a 250 mL round-bottom flask while being stirred at room temperature. At 80 °C, the mixture would be refluxed for 16 h. The excess Br_2 was then carefully rinsed away with deionized water (DI water) after cooling to room temperature. This produced white powder. Re-crystallizing the obtained solid from xylene would yield pure Th-Br_4 (2 g, 60%, Scheme S1). FTIR (KBr, Fig. S1): 3064 (aromatic C-H), 1552 (C═C), 590 (C-Br). ^{1}H NMR (500 MHz, Fig. S2): 7.98.

2.4. Synthesis of 2,8-dibromothianthrene (Tha-Br_2)

Th (3.24 g, 15 mmol), Br_2 (6 mL), and AcOH (60 mL) were inserted into a 250 mL round-bottom flask. The combination was heated to 80 °C for 16 h. After cooling down to room temperature, add deionized water (DI water) into the solution to form a white solid. The obtained solid was then rinsed with 5% of $NaHCO_3$ sodium hydrogen carbonate solution and recrystallized from DCM and methanol to acquire pure Tha-Br_2 (2.76 g, 85%, Scheme S2). FTIR (Fig. S3): 3057.41 (C-H aromatic). ^{1}H NMR (500 MHz, Fig. S4): 7.69, 7.62, 7.32. ^{13}C NMR (125 MHz, Fig. S5): 137.64–122.49.

2.5. Synthesis of 2,8-dibromothianthrene-5,5,10,10-tetraoxide (BSu-Br_2)

At room temperature with stirring in 150 mL of a two-necked round-bottom flask was added Tha-Br_2 (1.87 g, 5 mmol), AcOH (40 mL), and H_2O_2 (50 mL). The combination was treated at 90 °C and stirred for 24 h. The obtained white solid from the filter was washed with 5% of $NaHCO_3$ several times. In order to acquire a high-purity monomer, the solid undergoes recrystallization from DCM and methanol (1.4 g, 80%, Scheme S2). FTIR (Fig. S6): 3063.56 (aromatic C-H), 1165.89 (SO_2). ^{1}H NMR (Fig. S7): 8.41–7.52.

2.6. Synthesis of TPE-Ph-Th CMP

1,4-Ph-B$(OH)_2$ (0.2 g, 1 mmol), TPE-Br_4 (0.31 g, 0.4 mmol), Th-Br_4 (0.21 g, 0.4 mmol), K_2CO_3 (0.2 g, 8 mmol) and $Pd(PPh_3)_4$ (0.05 g, 0.05 mmol) directly into the round bottom flask with DMF solution (20 mL). The mixture underwent reflux in the N_2 atmosphere at 120 °C for 3 days. After the reaction was completed, the solution was filtered by THF, acetone, and MeOH to remove unreacted monomers. The obtained residue was then dried at 100 °C overnight to get light green powder [Fig. 1 **(a)**]: To prepare **TPE-Ph-Tha CMP:** DMF solution (20 mL), 1,4-Ph-B$(OH)_2$ (0.2 g, 1 mmol), TPE-Br_4 (0.31 g, 0.4 mmol), Tha-Br_2 (0.23 g, 0.6 mmol), K_2CO_3 (0.2 g, 8 mmol) and $Pd(PPh_3)_4$ (0.05 g, 0.05 mmol). The obtained solid was dried for one day under a vacuum at 110 °C in an oven to collect a light green solid [[Fig. 1**(b)**]: To prepare **TPE-Ph-BSu CMP** [Fig. 1**(c)**]: 1,4-Ph-B$(OH)_2$ (0.2 g, 1 mmol), TPE-Br_4 (0.31 g, 0.4 mmol), BSu-Br_2 (0.32 g, 0.6 mmol), K_2CO_3 (0.2 g, 8 mmol) and Pd$(PPh_3)_4$ (0.05 g, 0.05 mmol) in DMF (20 mL) to acquire the light green solid.

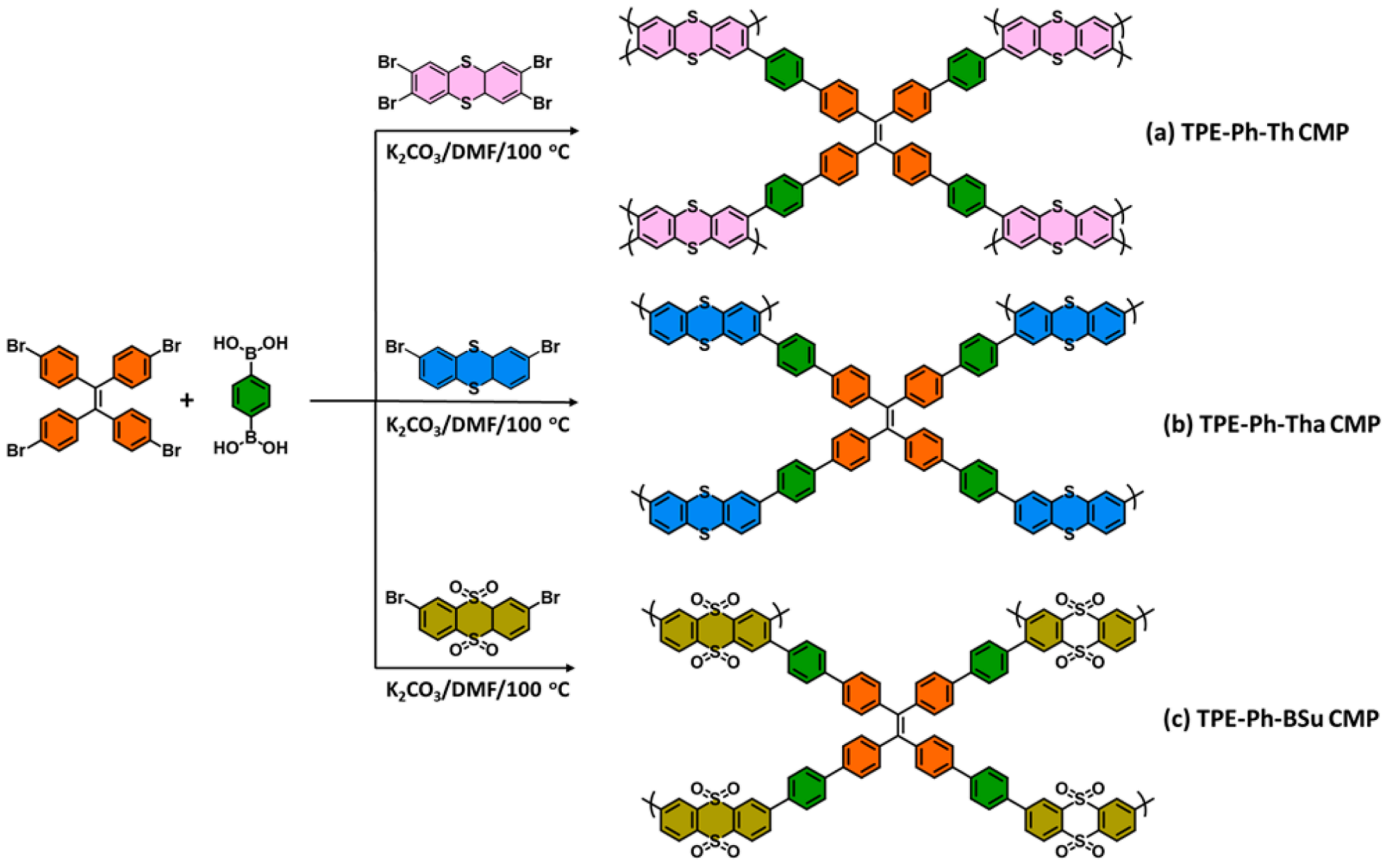

Fig. 1. The schematic approach for the synthesis of TPE-Ph-Th, TPE-Ph-Tha, and TPE-Ph-BSu CMPs.

3. Results and Discussion

3.1. Synthesis and Characterization of TPE-Ph-Th, TPE-Ph-Tha and TPE-Ph-BSu CMPs

In this study, four monomers, namely TPE-Br_4, Th-Br_4, Tha-Br_2, and BSu-Br_2, were prepared for the synthesis of three fluorescent TPE-Ph CMPs materials. These monomers were obtained through bromination and oxidation reactions, which were carried out on their respective starting materials. First, TPE was reacted for two days with excess Br_2 solution in the DCM/AcOH solution to create the TPE-Br_4 with a high yield. The Th-Br_4 was synthesized via the reaction of the Th compound with more amount of Br_2 under refluxing for 16 h in the AcOH solution [Scheme S1]. Also, Tha-Br_2 was prepared through the bromination reaction of the Th monomer, and then, Tha-Br_2 was reacted with the mixture of H_2O_2/AcOH to afford BSu-Br_2 [Scheme S2]. The spectroscopic analyses Th-Br_4, Tha-Br_2, and BSu-$Br_2$of and their data are provided and explained in the experimental part and supporting information file. Fig. 1 illustrates the synthesis of three new TPE-Ph CMPs incorporating TEP units via a Suzuki cross-coupling reaction. As depicted in Fig. 1, the light green solid was obtained by reacting Th-Br_4 or Tha-Br_2 or BSu-Br_2 with 1,4-Ph-B$(OH)_2$, TPE-Br_4, K_2CO_3, and Pd$(PPh_3)_4$ in a DMF solution to prepare TPE-Ph-Th [Fig. 1**(a)**], TPE-Ph-Tha [Fig. 1**(b)**], and TPE-Ph-BSu CMPs [Fig. 1**(c)**], respectively. The obtained TPE-Ph CMPs solids do not undecomposed and are insoluble in all organic solvents [acetone, DCM, EtOH, MeOH, and THF], revealing these TPE-Ph CMPs materials had been synthesized successfully and displayed high chemical stability also high crosslinking density [Figs. S8-S10]. To confirm the three novel TPE-Ph CMPs were successfully synthesized that all TPE-Ph CMPs would be tested by FTIR, ^{13}C solid-state NMR, and TGA analysis as provided in Fig. 2. All three TPE-Ph CMPs demonstrated the obvious absorption characteristics peaks around 3075 cm^{-1}, and 1610–1595 cm^{-1} in their FTIR spectra [Fig. 2 **(a)**] which represent the C-H aromatic and C= units; respectively. Furthermore, the ^{13}C NMR spectra of TPE-Ph-Th, TPE-Ph-Tha, and TPE-Ph-BSu CMPs [Fig. 2**(b)**] displayed clear signals from 119.32 to 90.04 ppm which represent aromatic carbon nuclei. To examine the thermal stability properties of TPE-Ph-Th, TPE-Ph-Tha, and TPE-Ph-BSu CMPs, all samples would be heated to 800 °C under N_2 atmosphere by thermogravimetric analysis (TGA) [Fig. 2**(c)**]. The declining thermal curve can be regarded as weight reduction, in other words, TGA can illuminate T_{d10} and char yield. As shown in TGA data the T_{d10} of TPE-Ph-Th, TPE-Ph-Tha, and TPE-Ph-BSu CMPs were 505, 462, and 535 °C, respectively. Moreover, the char yields at 800 °C for TPE-Ph-Th, TPE-Ph-Tha, and TPE-Ph-BSu CMPs were found to be 72, 63, and 73 wt%, respectively. The powder X-ray diffraction (PXRD) profile in Fig. 2**(d)**.

revealed that all three novel TPE-Ph CMPs materials exhibited an amorphous structure, as indicated by the presence of two broad peaks. XPS data confirmed the presence of both C and S atoms in both TPE-Ph-Th and TPE-Ph-Tha CMPs, while the TPE-Ph-BSu CMP exhibited the presence of C, S, and O atoms, as depicted in Fig. 3.

To identify the porosity properties of three TPE-Ph CMPs, each material was tested with nitrogen adsorption-desorption measurements at 77 K [Fig. 4]. Before the measurement, the TPE-Ph CMPs materials were

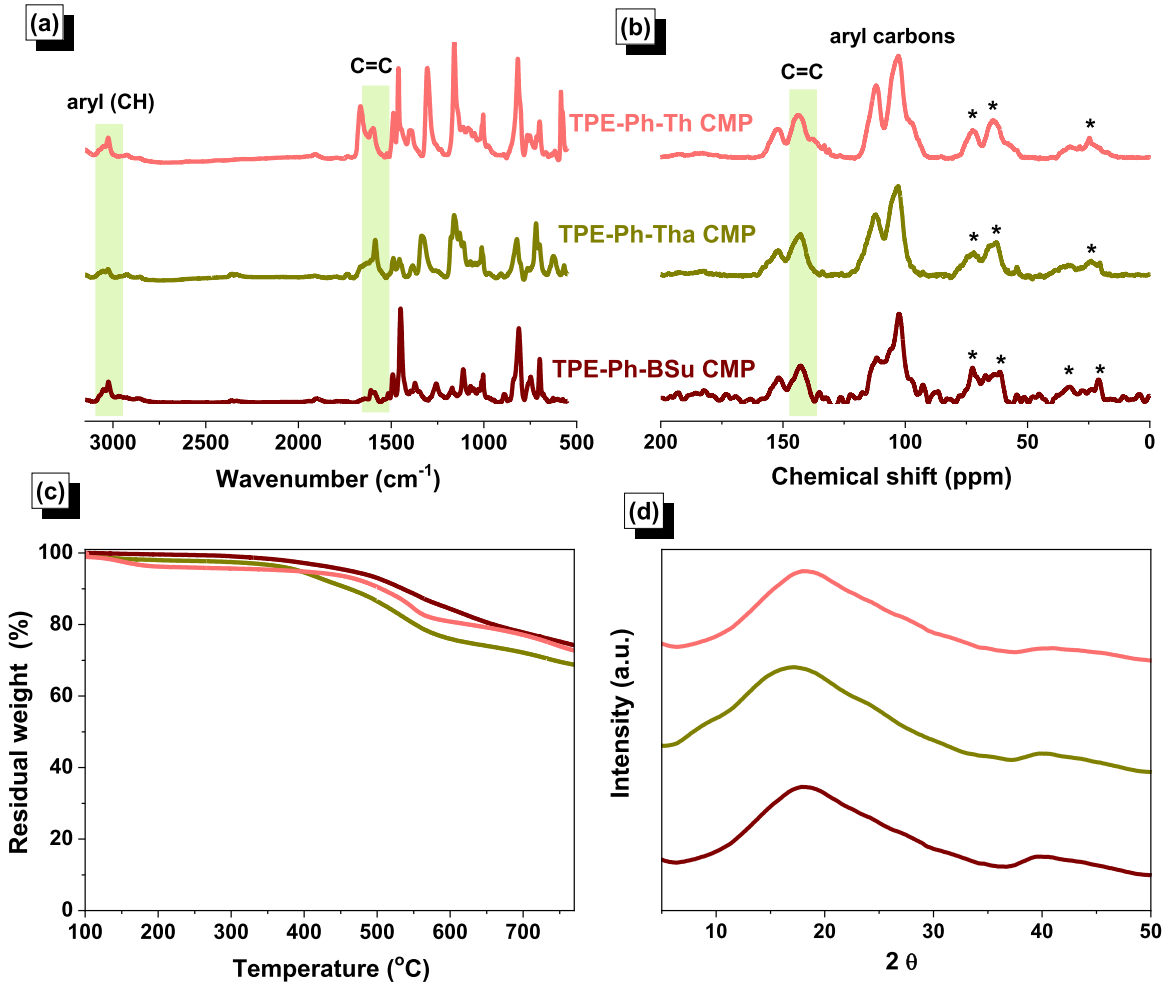

Fig. 2. The characterization data through (a) FTIR, (b) ss^{13}C NMR, (c) TGA, and (d) XRD of TPE-Ph-Th, TPE-Ph-Tha, and TPE-Ph-BSu CMPs.

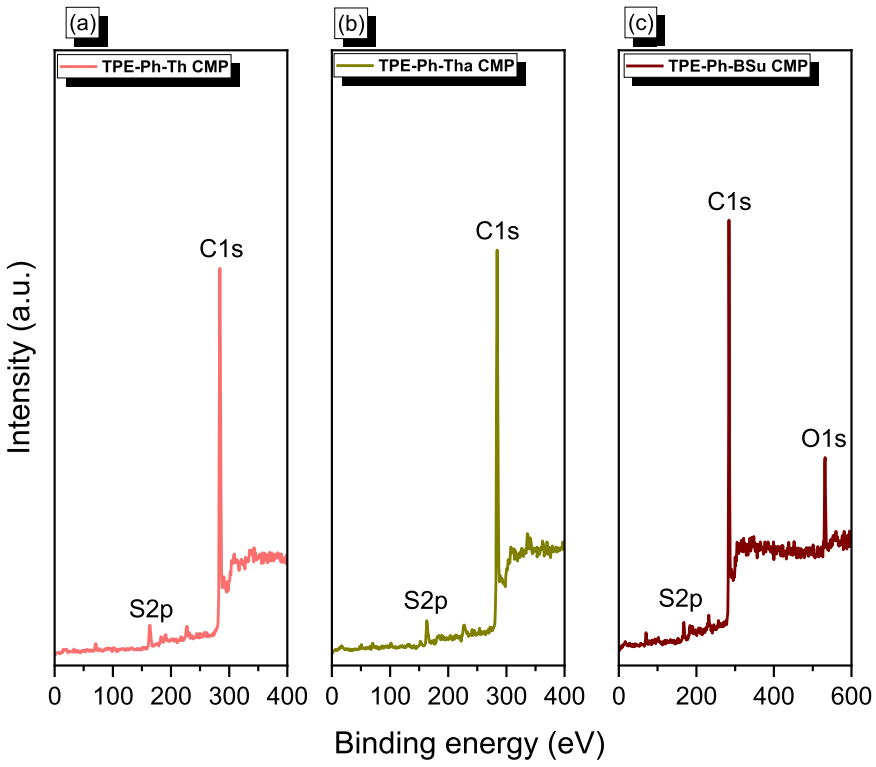

Fig. 3. XPS profiles of (a) TPE-Ph-Th, (b) TPE-Ph-Tha, and (c) TPE-Ph-BSu CMPs.

degassed under vacuum for 12 h at 150 °C. Among these three TPE-Ph CMPs materials all performed an instant increase for N_2 capture in $P/P_0 > 0.8$ shown in the N_2 adsorption-desorption profile [Fig. 4**(a-c)**]. In addition, the N_2 isotherms of three TPE-Ph CMPs confirmed that Type III (according to IUPAC classification) which indicated that the framework structure of TPE-Ph CMPs displayed microporous characteristics. The non-closure of the desorption curve for TPE-Ph-Tha CMP can be ascribed to the capillary condensation effect within its pore structure, leading to a delay when compared to the adsorption curve. The specific surface areas for TPE-Ph-Th, TPE-Ph-Tha, and TPE-Ph-BSu CMPs were 67, 18, and 41 $m^2\ g^{-1}$, respectively.

As for total pore volume (V_{total}) which was estimated from the N_2 absorbed when $P/P_0 = 0.99$ were 0.33, 0.1, and 0.1255 $cm^3\ g^{-1}$, respectively. Fig. 4**(d-f)** indicated the pore size diameter of TPE-Ph-Th, TPE-Ph-Tha, and TPE-Ph-BSu CMPs were 2, 2.6, and 2.1 nm, respectively. The TEM images in Fig. 5**(a-c)** demonstrated that all three TPE-Ph CMPs possessed a nano-porous network structure. The SEM images in Fig. 5**(d-f)** revealed that the surface morphologies of the three TPE-Ph CMPs exhibited an irregular and aggregated morphology. The elemental area mapping of TPE-Ph-Th and TPE-Ph-Tha CMPs using energy-dispersive X-ray spectroscopy (EDS) revealed a uniform distribution of carbon (C) and sulfur (S) atoms within their frameworks [Figs. S11**(a-f)**]. Additionally, the EDS results indicated that the TPE-Ph-BSu CMP material exhibited a homogeneous distribution of C, O, and S atoms [Figs. S11**(g-i)**].

3.2. Electrochemical Analysis of TPE-Ph-Th, TPE-Ph-Tha and TPE-Ph-BSu CMPs

In this investigation, a three-electrode setup with a 1.0 M KOH electrolyte was used to test the ability of three distinct samples, TPE-Ph-Th, TPE-Ph-Tha, and TPE-Ph-BSu CMPs, to store energy. The effectiveness of the samples was evaluated using the cyclic voltammetry (CV) and galvanostatic charge/discharge (GCD) tests within the working potential range of 0 to − 1.0 V. Fig. 6**(a-c)** present the CV of TPE-Ph-Th, TPE-Ph-Tha and TPE-Ph-BSu CMPs, respectively, measured at various scan rates (5–200 mV/s). These CV curves have specific redox characteristics and rectangular forms, indicating the significant contribution of both electrical double-layer capacitance (EDLC) and pseudocapacitance [66–70]. Additionally, it can be observed that the enclosed area of the curves expands with increasing scan rates, indicating improved capability. Fig. 6**(d-f)** display the GCD curves TPE-Ph-Th, TPE-Ph-Tha, and TPE-Ph-BSu CMPs from 0.5 to 20 A/g. The obtained samples exhibit triangular profiles with slight bends at 0.5 A/g, suggesting good reversibility of charge/discharge cycles and excellent capacitive behavior. Notably, the discharge time for all samples is longer than the charging time, indicating increased capacitance.

The calculations for the EDLC and pseudocapacitance contributions of TPE-Ph-Th, TPE-Ph-Tha, and TPE-Ph-BSu CMPs are depicted in Fig. 7. Our results indicate that the TPE-Ph-Th, TPE-Ph-Tha, and TPE-Ph-BSu CMPs exhibit pseudocapacitive contributions of 87.1%, 97.1%, and 99.5%, respectively.

Fig. 8**(a)** summarizes the specific capacitance values of all TPE-Ph CMP samples measured from 0.5 to 20 A/g using equation S1. The TPE-Ph-Th CMP exhibits specific capacitance values of 39.45, 5.46, 4.92, 4.38, 4.05, 3.85, 3.8, 3.6, and 3.6 $F\ g^{-1}$; TPE-Ph-Tha CMP demonstrates specific capacitance values of 51, 10.6, 9, 8.5, 7.75, 7.21, 6.8, 6.6, and 6.6 $F\ g^{-1}$, while TPE-Ph-BSu CMP achieves specific capacitance values of 52, 9.6, 7.88, 6.7, 6.53, 6.5, 6.2, 5.97, and 4.98 $F\ g^{-1}$. under various current densities of 0.5–20 A/g, respectively. Fig. 8**(b)** illustrates the cycling stability of each sample over consecutive 5000 cycles at 10 A/g. Remarkably, TPE-Ph-Th, TPE-Ph-Tha, and TPE-Ph-BSu CMPs demonstrate superior capacitance retention of 65%, 78%, and 80%, respectively. These values confirm the long-term stability and excellent cyclic capability of the samples, making them suitable for use as supercapacitor electrodes. Additionally, significant parameters such as energy and power densities for the samples are explored in Fig. 8**(c)**. Notably, TPE-Ph-Th, TPE-Ph-Tha, and TPE-Ph-BSu CMPs achieve energy densities of 5.5, 7.1, and 7.2 Wh/kg, respectively, at a power density of 250 W/kg. These values represent preferable performance

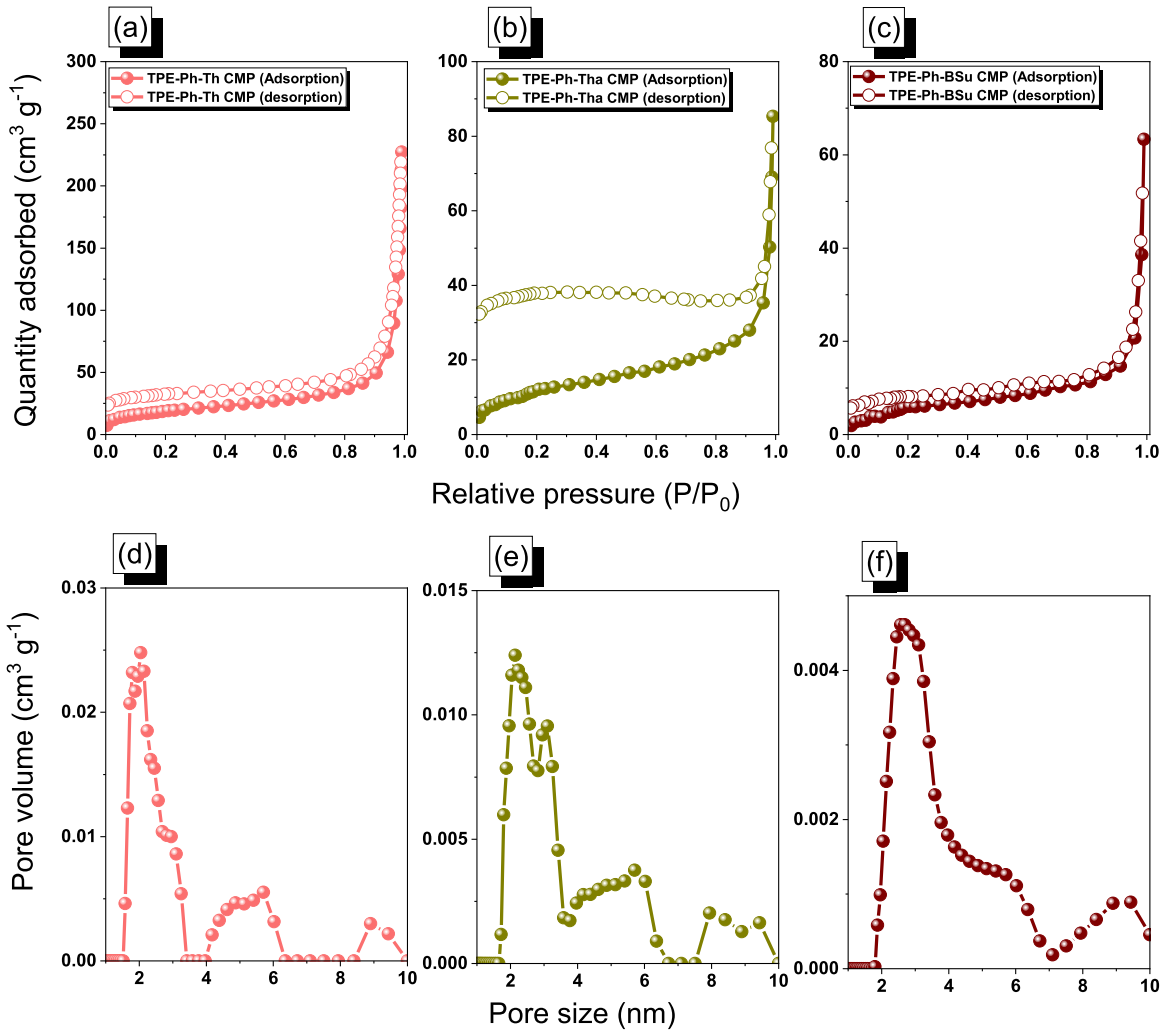

Fig. 4. The N_2 adsorption-desorption (a-c) and pore diameter (d-f) curves of (a, d) TPE-Ph-Th, (b, e) TPE-Ph-Tha, and (c, f) TPE-Ph-BSu CMPs.

characteristics for energy storage applications. Table S1 compares the specific capacitance of TPE-Ph-Th, TPE-Ph-Tha, and TPE-Ph-BSu CMPs with that of materials previously reported for supercapacitor (SC) applications.

3.3. Fluorescence properties and fluorescent sensing of p-nitrophenol for TPE-Ph-Th, TPE-Ph-Tha, and TPE-Ph-BSu CMPs

To explore the optical nature of the synthesized compounds namely TPE-Ph-Th, TPE-Ph-Tha, and TPE-Ph-BSu CMPs, they were submerged in various organic solvents such as EtOH, acetone, DMF, and THF, and their emission spectrum was recorded using a fluorescence spectrophotometer (Edinburg Instrument model FS5). As a result, TPE-Ph-Th CMP, TPE-Ph-Tha CMP, and TPE-Ph-BSu CMP exhibit significant fluorescence intensity between 510 nm and 530 nm range at different solvents mentioned above, as illustrated in Fig. 9, S12, and S13. In addition, beginning at excitation 300–400 nm, the obtained emission was highly dependent on excitation intensity, which was remarkably comparable to other frequently reported fluorescence and RTP-based nanoprobes utilized for various applications [71–73]. TPE-Ph-BSu CMP had an emission peak maximum at 530 nm, while TPE-Ph-Tha and TPE-Ph-Th CMPs had emission peak maximums at 517 nm and 527 nm, respectively (PL spectra showed in Figs. S12 and S13). THF mixed compounds show a maximum emission peak for all substances than that of the other solvents. This observation shows that the synthesized compounds' PL emission may be caused by localized sp2 carbon/sulfur subdomains (core state). Because of their distinct and individual excitation properties, the current probes exhibited a strong greenish-yellow fluorescence color.

The Commission Internationale de L'Eclairage (CIE) chromaticity diagram color chart in Fig. 10**, S14, and S15** show many points that suggest TPE-Ph-Th CMP, TPE-Ph-Tha CMP, and TPE-Ph-BSu CMP produce strong green fluorescence at excitation 340 nm. For all solvents, acetone and EtOH, however, displayed fewer x, y coordinates in the green light zone than they exhibited in the yellow region [Figs. 10**(a) and** 10**(c)**]. the PL emission of TPE-Ph-Th CMP covers the green-to-yellow edge (greenish-yellow) light area. The DMF and THF solvents' x, y coordinates primarily displayed a green zone that later stretched to a yellow region [Figs. 10**(b) and** 10**(d)**]. For DMF and THF, the TPE-Ph-Tha CMP instance exhibits a blue edge to the green area [Fig. S14**(b) and S14(d)**]. Only the green light portion of the screen displayed the x, y coordinates for the

solvent's acetone and EtOH [Fig. S14**(a) and S14(c)**]. The CIE (x,y) coordinates chromaticity diagram in Figs. S15**(a)-S15(d)** shows that all of the solvents for TPE-Ph-BSu CMP had similar types of x,y coordinates at green light areas. The quantum yields (QY) for TPE-Ph-Th, TPE-Ph-Tha, and TPE-Ph-BSu CMPs were 7.58%, 1.26%, and 3.34%, respectively. The electron-deficient nitroaromatic compounds (NACs) are capable of interacting noncovalently with electron-rich aromatic rings, resulting in alterations to the fluorescence emission characteristics of the fluorophore. One example of such changes can be seen in the well-known thermal stability and -conjugated skeletons based on TPE. The

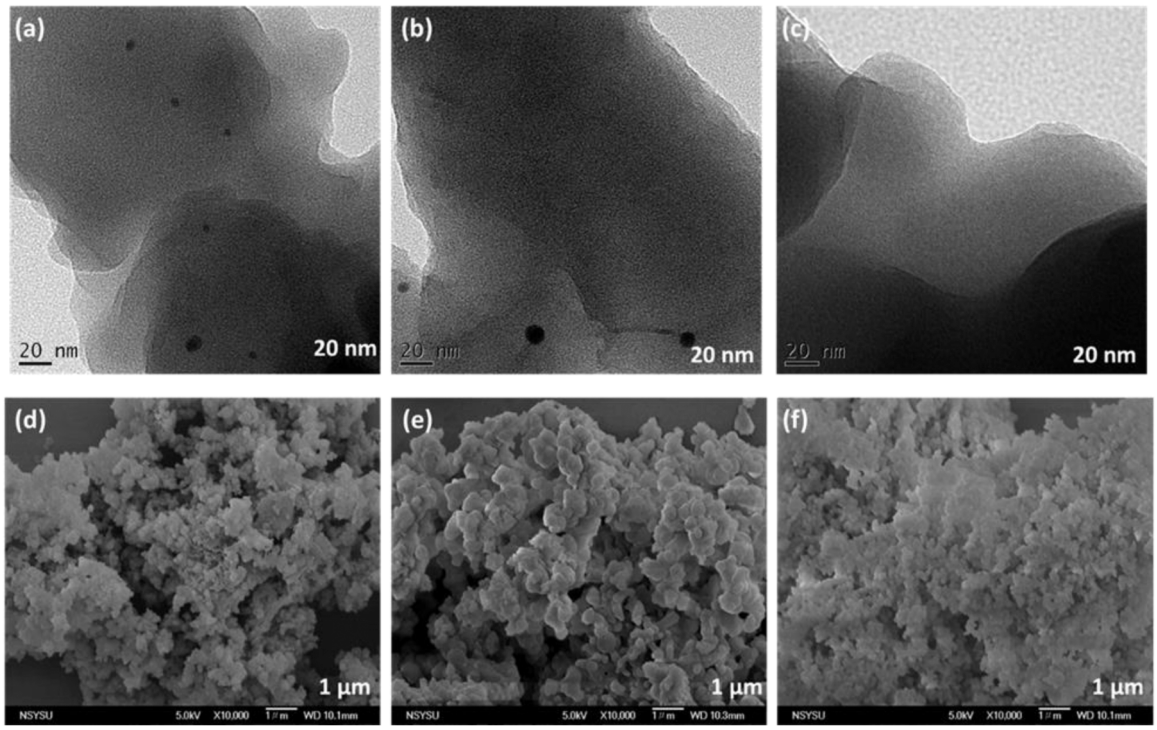

Fig. 5. HR-TEM (a-c) and SEM (d-f) images of (a, d) TPE-Ph-Th, (b, e) TPE-Ph-Tha, and (c, f) TPE-Ph-BSu CMPs.

direct attachment of the thiophene moiety to the phenyl ring system imparts high rigidity, which effectively prevents the occurrence of significant π − π stacking interactions and helps to minimize aggregation-caused quenching (ACQ) [74,75]. Due to the potential for stronger noncovalent interactions between PNP and TPE-Ph- CMPs FL probes, a noticeable enhancement in quenching by PNP has been observed. Under the optimal experimental circumstances, the effect of the PNP on the fluorescence of the TPE-Ph-Th CMP, TPE-Ph-Tha CMP, and TPE-Ph-BSu CMP has been evaluated. To sense the PNP, different concentrations of PNP were prepared and their fluorescence intensity was monitored at 530 nm, 517 nm, and 527 nm with the fixed excitation [Fig. 11**]** to assess the sensitivity of the prepared compounds TPE-Ph-Th CMP, TPE-Ph-Tha CMP, and TPE-Ph-BSu CMP for detecting PNP. Fig. 11**(a-c) depict** the influence of PNP concentration (5×10^{-6} to 1×10^{-2} M) on TPE-Ph-Th CMP, TPE-Ph-Tha CMP, and TPE-Ph-BSu CMP emission spectra. (F_0-F)/F decreased linearly with PNP concentration increased from 5×10^{-6} to 1×10^{-4} M in Fig. S16, with a calibration function of (F_0-F)/F = 0.0341 C_{PNP} - 0.0088 and a correlation value (R^2) of 0.97 for TPE-Ph-Th CMP. (F_0-F)/F rise linearly with PNP concentration raises from 5×10^{-6} to 1×10^{-4} M in Fig. S16**(a)**, with a calibration function of (F_0-F)/F = 0.051 C_{PNP} - 0.0116 and a correlation value (R^2) of 0.92 for TPE-Ph-Tha CMP [Fig. S16**(b)**]. For TPE-Ph-BSu CMP the (F_0-F)/F was raised linearly with PNP concentration raises from 5×10^{-6} to 1×10^{-4} M in Fig. S16**(c)**, with a calibration function of (F_0-F)/F = 0.0429 C_{PNP} - 0.00986 and a correlation value (R^2) of 0.97. The detection limits for PNP were determined as follows: 4.3×10^{-8} M for TPE-Ph-Th CMP, 4.7×10^{-8} M for TPE-Ph-Tha CMP, and 5.1×10^{-8} M for TPE-Ph-BSu CMP. Our sensing method exhibited a high degree of comparability with previously reported PNP sensing methods (Table S2). All synthesized compounds act as good fluorescent probes for the detection of PNP at a trace level. However, high linearity was observed on the TPE-Ph-BSu CMP probe for the detection of PNP. It is due to the functional group on the surface of TPE cored CMP molecule.

In order to craft a probe with exceptional selectivity and sensitivity, it is imperative to possess a comprehensive understanding of the interplay among the molecular structures of the probe, quencher, and the fluorescence quenching process. Photoinduced electron transfer (PET) is a phenomenon characterized by the migration of electrons from a donor with an electron surplus to an acceptor with an electron deficit. For this intricate dance to transpire, the energy differential between the highest occupied molecular orbital (HOMO) and the lowest unoccupied molecular orbital (LUMO) of the probe must surpass the disparity between the LUMO levels of the probe (donor) and the quencher (acceptor). Furthermore, it's worth noting that PNP possesses a robust light-absorption capacity within the wavelength range of 200–450 nm. Particularly noteworthy is the alignment of PNP's absorption band with the emission wavelength (excitation) at 527 nm, 519 nm, and 531 nm, respectively. Consequently, competition emerges between the emission band of the fluorescent molecule and the absorption band of the analyzed substance, culminating in the effective quenching of PNP. The quenching of luminescence in PNP (as illustrated in Fig. 12) can be attributed to the transfer of electrons from the electron-rich probe to the electron-deficient PNP molecules. When PNP infiltrates the probe environment, the presence of robust π-stacking interactions and other favorable interactions substantially heightens the efficacy of quenching [65].

The extraordinary aggregation-induced emission properties displayed by the synthesized TPE-Ph-Th, TPE-Ph-Tha, and TPE-Ph-BSu CMPs further inspired us to investigate the sensing potential of PNP. TPE has rotating peripheral aromatic rings and a distinctive propeller-shaped structure. It is widely known that the system's thianthrene moiety's strong rigidity successfully resists stacking interactions (π − π), preventing aggregation-induced quenching. The energy transfer mechanism between TPE-Ph-Th, TPE-Ph-Tha, and TPE-Ph-BSu CMPs and PNP that occurs when PNP is added to the CMPs intensifies the fluorescence quenching effect. The fluorescence decay spectra were observed when excited at 365 nm for TPE-Ph-Th, TPE-Ph-Tha, and TPE-Ph-BSu CMPs with PNP. These spectra were analyzed using biexponential curve fitting, resulting in average lifetimes of 5.81 ns, 6.10 ns, and 4.54 ns for TPE-Ph-Th, TPE-Ph-Tha, and TPE-Ph-BSu CMPs, respectively [Fig. S17]. Due to their remarkable fluorescence characteristics, the TPE-Ph-Th, TPE-Ph-Tha, and TPE-Ph-BSu CMPs exhibit great potential for application as chemical sensors capable of detecting various metal ions. In the context of this chemical sensing study, a diverse range of metal ions was

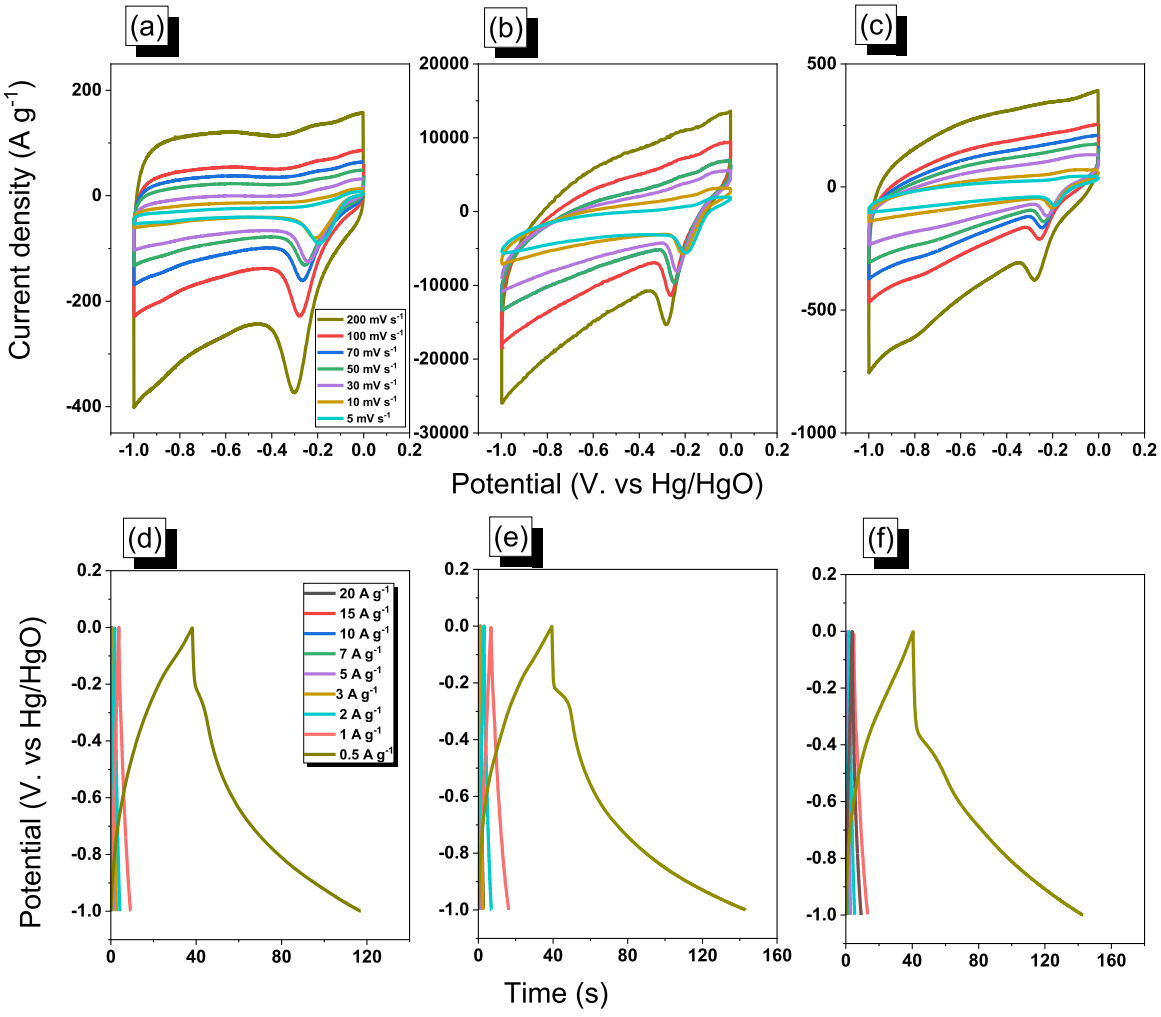

Fig. 6. Corresponding CV (a-c) and GCD (d-f) profiles of (a, c) TPE-Ph-Th, (b, d) TPE-Ph-Tha, and (c, f) TPE-Ph-BSu CMPs.

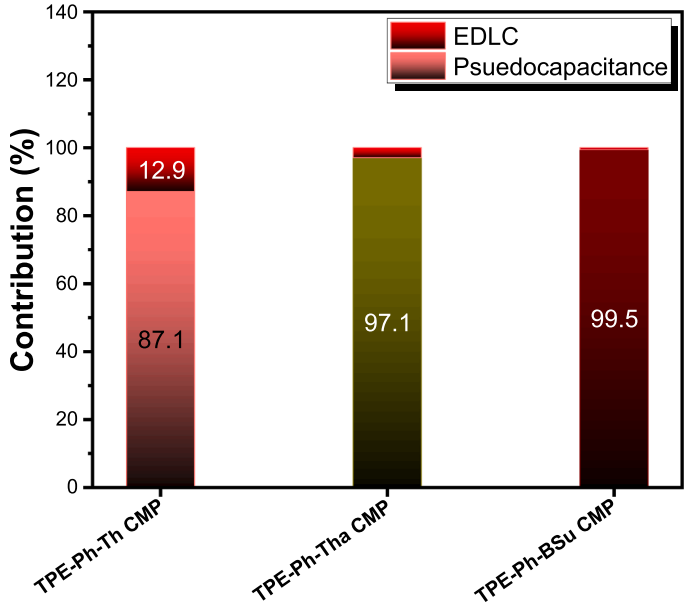

Fig. 7. EDLC and pseudocapacitance contribution of TPE-Ph-Th, TPE-Ph-Tha, and TPE-Ph-BSu CMPs.

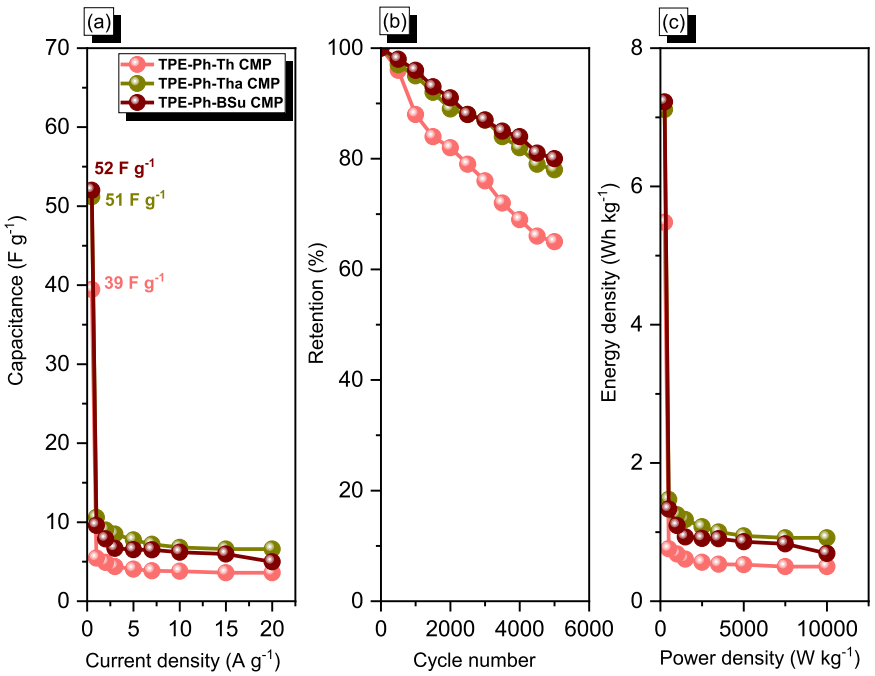

Fig. 8. Corresponding capacitance (a), capacitance retention (b), and Ragone (c) profiles of TPE-Ph-Th, TPE-Ph-Tha, and TPE-Ph-BSu CMPs.

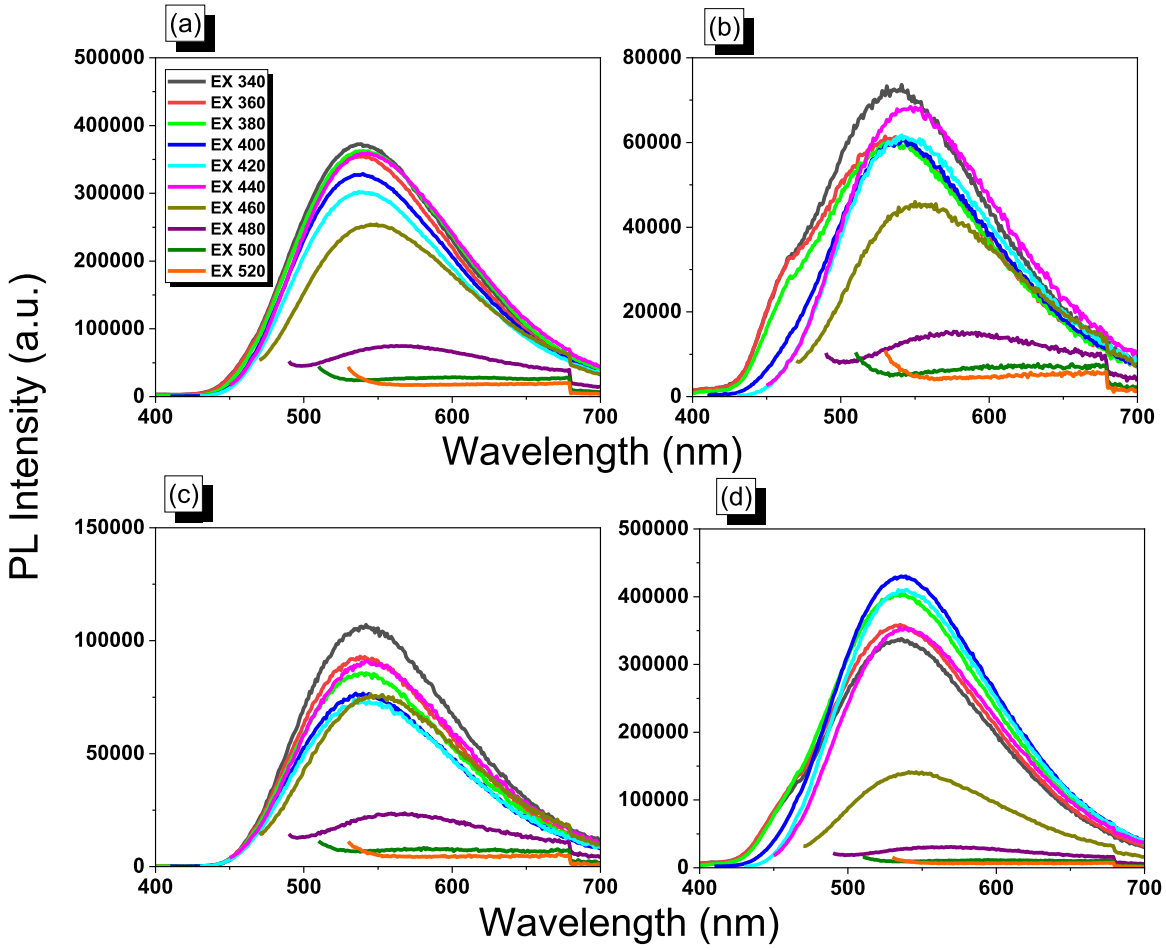

Fig. 9. Fluorescence spectra of the TPE-Ph-Th CMP in (a) acetone, (b) DMF, (c) EtOH, and (d) THF.

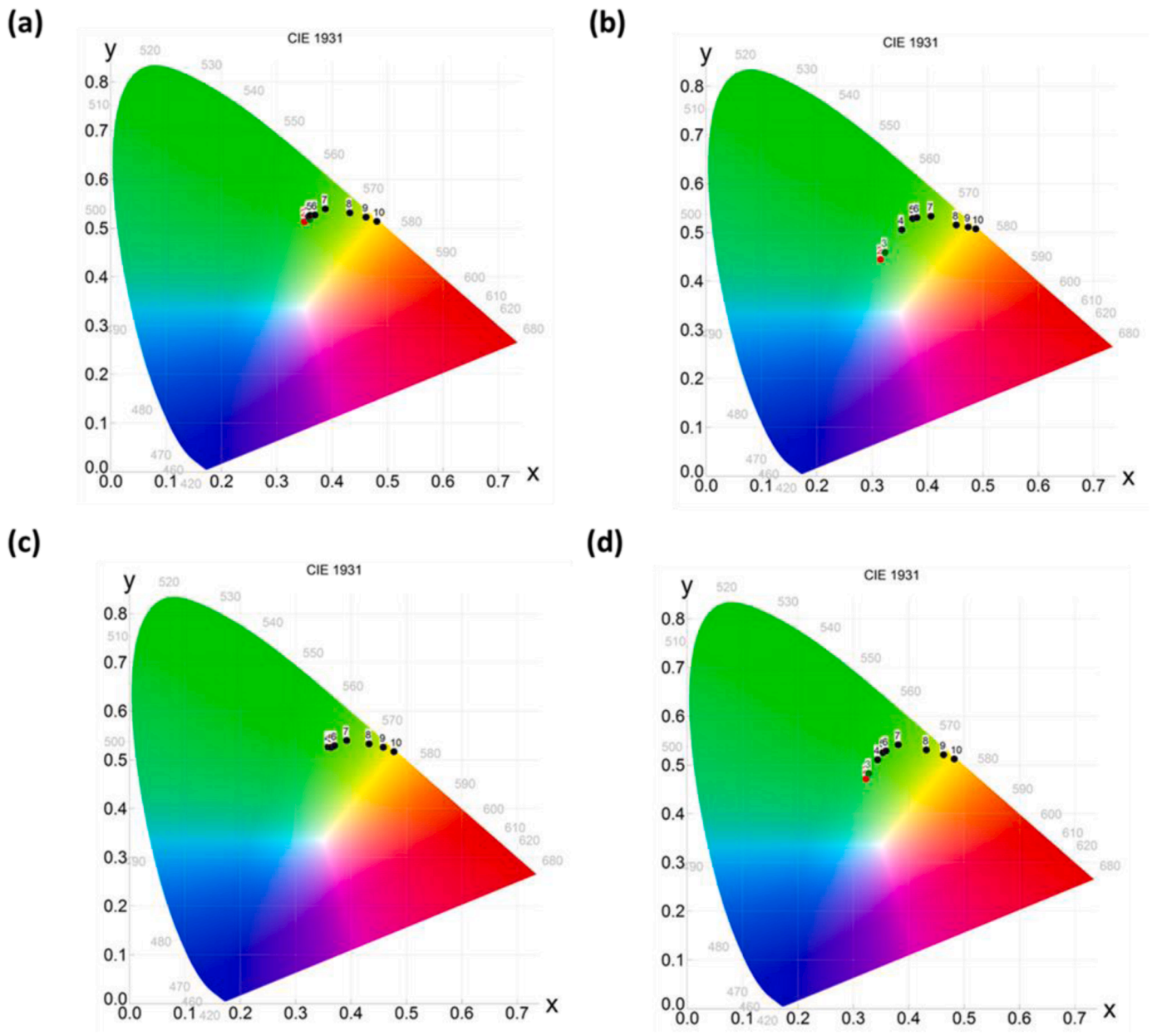

Fig. 10. The effect on CIE chromaticity diagram of the TPE-Ph-Th CMP at different solvents (a) acetone (b) DMF, (c) EtOH and (d) THF.

deliberately chosen to serve as interfering analytes, encompassing Co^{2+}, Cr^{3+}, Cu^{2+}, Fe^{2+}, Hg^{2+}, Pb^{2+}, and Zn^{2+} ions. Upon introducing these metal ions at a concentration of 0.01 mol/L (2 mL) into a 2 mL dispersion of CMPs (TPE-Ph-Th, TPE-Ph-Tha, and TPE-Ph-BSu), which were prepared by dispersing 4 mg of the CMPs in 10 mL of tetrahydrofuran (THF), an intriguing observation emerged. The outcomes of our study are visually represented in Figs. S18, S19, and S20. Figs. S18, S19, and S20 vividly illustrate the variation in peak intensity at 530 nm, 517 nm, and 527 nm concerning TPE-Ph-Th, TPE-Ph-Tha, and TPE-Ph-BSu CMPs when exposed to a range of metal ions, including Co^{2+}, Cr^{3+}, Cu^{2+}, Fe^{2+}, Hg^{2+}, Pb^{2+}, and Zn^{2+}. Remarkably, the plotted data reveals that the emission intensity of the CMPs remained unaltered, and no substantial quenching was observed. This finding underscores the resilience and reliability of these materials as chemical sensors tailored for the detection of the aforementioned metal ions. Our study distinctly establishes the exceptional selectivity of TPE-Ph-Th, TPE-Ph-Tha, and TPE-Ph-BSu CMPs in detecting PNP without any interference from other substances.

4. Conclusions

In our recent study, we successfully synthesized a unique set of TPE-Ph linked CMPs through a straightforward Suzuki cross-coupling reaction. This reaction involved the use of Th-Br_4 or Tha-Br_2 or BSu-Br_2, along with 1,4-Ph-$B(OH)_2$ and TPE-Br_4, in a DMF solvent. Among the three TPE-Ph CMP materials synthesized, the TPE-Ph-BSu CMP material exhibited the most favorable thermal characteristics, with a T_{d10} value of 535 °C and a char yield of 73 wt%. Furthermore, we explored the application of the TPE-Ph CMP materials as electrode-active materials for SCs. Both TPE-Ph-Tha and TPE-Ph-BSu CMPs demonstrated excellent supercapacitive activity in our electrochemical experiments. Specifically, their specific capacities were measured to be 51 and 52 F g^{-1}, respectively, at 0.5 A g^{-1}. Additionally, the TPE-Ph-Tha and TPE-Ph-BSu CMPs exhibited remarkable capacitance retention, retaining 80% of their initial capacitance after undergoing 5000 charge-discharge cycles. Moreover, we have successfully employed the three TPE-Ph CMPs-based fluorophores for the detection of PNP. Among the three CMPs,

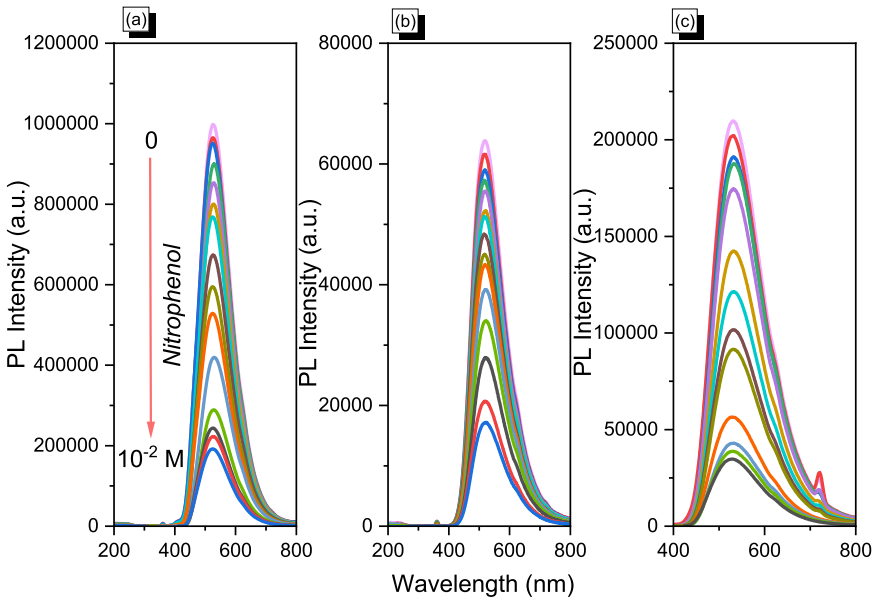

Fig. 11. Fluorescence spectra of the TPE-Ph-Th, TPE-Ph-Tha, and TPE-Ph-BSu CMPs by adding various concentrations of PNP (0–10^{-2} M, λ_{ex} = 365 nm).

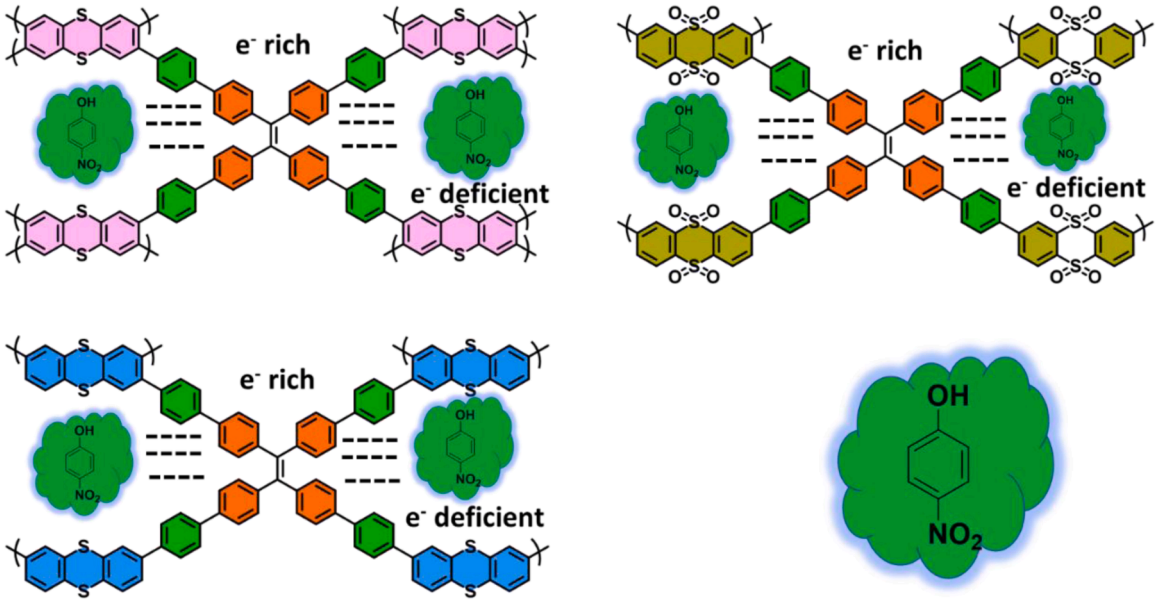

Fig. 12. Schematic cartoon for the quenching fluorescence mechanism of the TPE-Ph-Th, TPE-Ph-Tha, and TPE-Ph-BSu CMPs towards *p*-nitrophenol.

TPE-Ph-BSu CMP exhibited superior sensitivity compared to the others. This improved sensitivity can be attributed to the favorable electron-transferring energy level matching achieved through the phenomenon of PICT.

CRediT authorship contribution statement

Mohamed Gamal Mohamed: Investigation, Methodology, Conceptualization, Supervision, Writing – original draft. **Huan-Yu Hu:** Investigation, Methodology. **S. Santhoshkumar:** Investigation, Writing – original draft. **Manivannan Madhu:** Investigation, Methodology. **Tharwat Hassan Mansoure**: Investigation. **Ching-Wen Hsiao:** Investigation. **Yunsheng Ye:** Investigation. **Cheng-Wei Huang:** Investigation. **Wei-Lung Tseng:** Supervision. **Shiao-Wei Kuo:** Supervision.

Declaration of Competing Interest

The authors declare that they have no known competing financial interests or personal relationships that could have appeared to influence the work reported in this paper.

Data Availability

The data that has been used is confidential.

Acknowledgments

This study was supported financially by the Ministry of Science and Technology, Taiwan, under contracts NSTC 110–2124-M-002–013 and 111–2223-E-110–004. The authors thank the staff at National Sun Yat-sen University for their assistance with the TEM (ID: EM022600)

experiments.

Appendix A. Supporting information

Supplementary data associated with this article can be found in the online version at doi:10.1016/j.colsurfa.2023.132675.

References

[1] M.G. Mohamed, S.V. Chaganti, M.S. Li, M.M. Samy, S.U. Sharma, J.T. Lee, M. H. Elsayed, H.H. Chou, S.W. Kuo, Ultrastable porous organic polymers containing thianthrene and pyrene units as organic electrode materials for supercapacitors, ACS Appl. Energy Mater. 5 (2022) 6442–6452, https://doi.org/10.1021/acsaem.2c00942.

[2] M.G. Mohamed, H.-Y. Hu, M. Madhu, M. Ejaz, S.U. Sharma, W.L. Tseng, M. M. Samy, C.W. Huang, J.T. Lee, S.W. Kuo, Construction of ultrastable conjugated microporous polymers containing thiophene and fluorene for metal ion sensing and energy storage, Micromachines 13 (2022) 1466, https://doi.org/10.3390/mi13091466.

[3] M.M. Samy, M.G. Mohamed, A.F.M. El-Mahdy, T.H. Mansoure, K.C.W. Wu, S. W. Kuo, High-performance supercapacitor electrodes prepared from dispersions of tetrabenzonaphthalene-based conjugated microporous polymers and carbon nanotubes, ACS Appl. Mater. Interfaces 13 (2021) 51906–51916, https://doi.org/10.1021/acsami.1c05720.

[4] M.G. Mohamed, T.H. Mansoure, M.M. Samy, Y. Takashi, A.A.K. Mohammed, T. Ahamad, S.M. Alshehri, J. Kim, B.M. Matsagar, K.C.W. Wu, S.W. Kuo, Ultrastable conjugated microporous polymers containing benzobisthiadiazole and pyrene building blocks for energy storage applications, Molecules 27 (2022) 2025, https://doi.org/10.3390/molecules27062025.

[5] S. Zheng, Q. Li, H. Xue, H. Pang, Q. Xu, A highly alkaline-stable metal oxide@metal−organic framework composite for high-performance electrochemical energy storage, Natl. Sci. Rev. 7 (2020) 305–314, https://doi.org/10.1093/nsr/nwz137.

[6] S. Najib, E. Erdem, Current progress achieved in novel materials for supercapacitor electrodes: mini review, Nanoscale Adv. 1 (2019) 2817–2827, https://doi.org/10.1039/C9NA00345B.

[7] C. Liu, Y. Bai, W. Li, F. Yang, G. Zhang, H. Pang, In Situ Growth of Three-Dimensional MXene/Metal–Organic Framework Composites for High-Performance Supercapacitors. Angew. Chem, Int. Ed. 61 (2022), e202116282, https://doi.org/10.1002/anie.202116282.

[8] S. Liu, L. Kang, J. Henzie, J. Zhang, J. Ha, M.A. Amin, M.S.A. Hossain, S.C. Jun, Y. Yamauchi, Recent Advances and Perspectives of Battery-Type Anode Materials for Potassium Ion Storage, ACS Nano 15 (2021) 18931–18973, https://doi.org/10.1021/acsnano.1c08428.

[9] N.S. Shaikh, S.B. Ubale, V.J. Mane, J.S. Shaikh, V.C. Lokhande, S. Praserthdam, C. D. Lokhande, P. Kanjanaboos. Novel electrodes for supercapacitors: Conducting polymers, metal oxides, chalcogenides, carbides, nitrides, MXenes, and, their Compos. Graph. J. Alloy. Compd. 893 (2022) 61998, https://doi.org/10.1016/j.jallcom.2021.161998.

[10] S. Zheng, Y. Sun, H. Xue, P. Braunstein, W. Huang, H. Pang, Dual-ligand and hard-soft-acid-base strategies to optimize metal-organic framework nanocrystals for stable electrochemical cycling performance, Natl. Sci. Rev. 9 (2022) nwab197, https://doi.org/10.1093/nsr/nwab197.

[11] A.O. Mousa, Z.I. Lin, C.H. Chuang, C.K. Chen, S.W. Kuo, M.G. Mohamed, Rational Design of Bifunctional Microporous Organic Polymers Containing Anthracene and Triphenylamine Units for Energy Storage and Biological Applications, Int. J. Mol. Sci. 24 (2023) 8966, https://doi.org/10.3390/ijms24108966.

[12] S.Y. Chang, A.M. Elewa, M.G. Mohamed, I.M.A. Mekhemer, M.M. Samy, K. Zhang, H.H. Chou, S.W. Kuo, Rational design and synthesis of bifunctional Dibenzo[g,p]chrysene-based conjugated microporous polymers for energy storage and visible light-driven photocatalytic hydrogen evolution, Mater. Today Chem. 33 (2023), 101680, https://doi.org/10.1016/j.mtchem.2023.101680.

[13] Y. Bai, C. Liu, T. Chen, W. Li, S. Zheng, Y. Pi, Y. Luo, H. Pang, MXene-Copper/Cobalt Hybrids via Lewis Acidic Molten Salts Etching for High Performance Symmetric Supercapacitors. Angew. Chem, Int. Ed. 60 (2021) 25318–25322, https://doi.org/10.1002/anie.202112381.

[14] M.G. Mohamed, H.Y. Hu, M. Madhu, M.M. Samy, I.M.A. Mekhemer, W.L. Tseng, H. H. Chou, S.W. Kuo, Ultrastable two-dimensional fluorescent conjugated microporous polymers containing pyrene and fluorene units for metal ion sensing and energy storage, Eur. Polym. J. 189 (2023), 111980, https://doi.org/10.1016/j.eurpolymj.2023.111980.

[15] M.M. Samy, M.G. Mohamed, S.W. Kuo, Conjugated Microporous Polymers Based on Ferrocene Units as Highly Efficient Electrodes for Energy Storage, Polymers 15 (2023) 1095, https://doi.org/10.3390/polym15051095.

[16] W. Septiani, Y.V. Kaneti, K.B. Fathoni, J. Wang, Y. Ide, B. Yuliarto, B. Nugraha, H. K. Dipojono, A.K. Nanjundan, D. Golberg, Y. Bando, Y. Yamauchi, Self-Assembly of Nickel Phosphate-Based Nanotubes into Two-Dimensional Crumpled Sheet-Like Architectures for High-Performance Asymmetric Supercapacitors, Nano Energy 67 (2020), 104270, https://doi.org/10.1016/j.nanoen.2019.104270.

[17] W. Lyu, C. Yan, Z. Chen, J. Chen, H. Zuo, L. Teng, H. Liu, L. Wang, Y. Liao, Spirobifluorene-Based Conjugated Microporous Polymer-Grafted Carbon Nanotubes for Efficient Supercapacitive Energy Storage, ACS Appl. Energy Mater. 5 (2022) 3706–3714, https://doi.org/10.1021/acsaem.2c00151.

[18] A.M. Khattak, H. Sin, Z.A. Ghazi, X. He, B. Liang, N.A. Khan, H.R. Alanagh, A. Iqbal, L.S. Li, Z.T. Tang, Controllable fabrication of redox-active conjugated microporous polymer on reduced graphene oxide for high performance faradaic energy storage, J. Mater. Chem. A 6 (2018) 18827–18832, https://doi.org/10.1039/C8TA07913G.

[19] L. Mei, J.C. Wei, Q. Duan, Construction of copper porphyrinlinked conjugated microporous polymer/carbon nanotube composite as flexible electrodes for supercapacitors, J. Mater. Sci. Mater. Electron 32 (2021) 24953–24963, https://doi.org/10.1007/s10854-021-06952-w.

[20] M.G. Mohamed, A.F.M. EL-Mahdy, M.G. Kotp, S.W. Kuo, Advances in porous organic polymers: Syntheses, structures, and diverse applications, Mater. Adv. 3 (2022) 707–733, https://doi.org/10.1039/D1MA00771H.

[21] G. Cai, P. Cui, W. Shi, S. Morris, S.N. Lou, J. Chen, J.H. Ciou, V.K. Paidi, K.S. Lee, S. Li, P.S. Lee, One-Dimensional π -d Conjugated Coordination Polymer for Electrochromic Energy Storage Device with Exceptionally High Performance, Adv. Sci. 7 (2020) 1903109, https://doi.org/10.1002/advs.201903109.

[22] D.H. Roh, H. Shin, H.T. Kim, T.H. Kwon, Sono-Cavitation and Nebulization-Based Synthesis of Conjugated Microporous Polymers for Energy Storage Applications, ACS Appl. Mater. Interfaces 13 (2021) 61598–61609, https://doi.org/10.1021/acsami.1c13755.

[23] M.G. Mohamed, E.C. Atayde Jr., M.B. Matsagar, J. Na, Y. Yamauchi, K.C.W. Wu, S. W. Kuo, Construction Hierarchically Mesoporous/Microporous Materials Based on Block Copolymer and Covalent Organic Framework, J. Taiwan Inst. Chem. Eng. 112 (2020) 180–192, https://doi.org/10.1016/j.jtice.2020.06.013.

[24] M.M. Samy, M.G. Mohamed, T.H. Mansoure, T.S. Meng, M.A.R. Khan, C.C. Liaw, S. W. Kuo, Solid state chemical transformations through ring-opening polymerization of ferrocene-based conjugated microporous polymers in host–guest complexes with benzoxazine-linked cyclodextrin, J. Taiwan Inst. Chem. Eng. 132 (2022), 104110, https://doi.org/10.1016/j.jtice.2021.10.010.

[25] Y. Tong, J. Yang, J. Li, Z. Cong, L. Wei, M. Liu, S. Zhai, K. Wang, Q. An, Lignin-derived electrode materials for supercapacitor applications: progress and perspectives, J. Mater. Chem. A 11 (2023) 1061–1082, https://doi.org/10.1039/d2ta07203c.

[26] X. Wang, W. Zhang, Q. Zhou, F. Ran, Integrating supercapacitor with sodium hyaluronate based hydrogel as a novel All-In-One wound Dressing: Self-Powered electronic stimulation, Chem. Eng. J. 452 (2023), 139491, https://doi.org/10.1016/j.cej.2022.139491.

[27] L. Hu, S. Gu, W. Yu, W. Zhang, Q. Xie, C. Pan, J. Tang, G. Yu, Facile preparation of CoO nanoparticles embedded N-doped porous carbon from conjugated microporous polymer for oxygen reduction reaction, J. Colloid Interface Sci. 562 (2020) 550–557, https://doi.org/10.1016/j.jcis.2019.11.079.

[28] M.M. Samy, M.G. Mohamed, S.U. Sharma, S.V. Chaganti, J.T. Lee, S.W. Kuo, An Ultrastable Tetrabenzonaphthalene-Linked conjugated microporous polymer functioning as a high-performance electrode for supercapacitors, J. Taiwan Inst. Chem. Eng. (2023), 104750, https://doi.org/10.1016/j.jtice.2023.104750.

[29] W. Zhang, Z. Deng, J. Deng, C.T. Hu, Y. Liao, H. Yang, Q. Liu, Regulating the exciton binding energy of covalent triazine frameworks for enhancing photocatalysis, J. Mater. Chem. A 10 (2022) 22419–22427, doi.org/10.1039/D2TA06479K. DOI: 10.1021/acsami.7b08060.

[30] H.L. Qian, C. Dai, C.X. Yang, X.P. Yan, High-crystallinity covalent organic framework with dual fluorescence emissions and its ratiometric sensing application, ACS Appl. Mater. Interfaces 9 (2017) 24999–25005.

[31] H. Bildirir, V.G. Gregoriou, A. Avgeropoulos, U. Scherf, C.L. Chochos, Porous organic polymers as emerging new materials for organic photovoltaic applications: current status and future challenges, Mater. Horiz. 4 (2017) 446–556, https://doi.org/10.1039/C6MH00570E.

[32] Y. Shi, N. Meng, Y. Wang, Z. Cheng, W. Zhang, Y. Liao, Scalable Fabrication of Conjugated Microporous Polymer Sponges for Efficient Solar Steam Generation, ACS Appl. Mater. Interfaces 14 (2022) 4522–4531, https://doi.org/10.1021/acsami.1c21693.

[33] M.G. Mohamed, W.C. Chang, S.W. Kuo, Crown Ether- and Benzoxazine-Linked Porous Organic Polymers Displaying Enhanced Metal Ion and CO_2 Capture through Solid-State Chemical Transformation, Macromolecules 55 (2022) 7879–7892, https://doi.org/10.1021/acs.macromol.2c01216.

[34] J. Kim, J.H. Kim, K. Ariga, Redox-Active Polymers for Energy Storage Nanoarchitectonics, Joule 1 (2017) 739–768, https://doi.org/10.1016/j.joule.2017.08.018.

[35] M.G. Mohamed, M.H. Elsayed, Y. Ye, M.M. Samy, A.E. Hassan, T.H. Mansoure, Z. Wen, H.H. Chou, K.H. Chen, S.W. Kuo, Construction of Porous Organic/Inorganic Hybrid Polymers Based on Polyhedral Oligomeric Silsesquioxane for Energy Storage and Hydrogen Production from Water, Polymers 15 (2023) 182, https://doi.org/10.3390/polym15010182.

[36] M.M. Samy, M.G. Mohamed, S.U. Sharma, S.V. Chaganti, T.H. Mansoure, J.T. Lee, T. Chen, S.W. Kuo, Constructing conjugated microporous polymers containing triphenylamine moieties for high-performance capacitive energy storage, Polymer 264 (2023), 125541, https://doi.org/10.1016/j.polymer.2022.125541.

[37] M.G. Mohamed, M.M. Samy, T.H. Mansoure, C.J. Li, W.C. Li, J.H. Chen, K. Zhang, S.W. Kuo, Microporous Carbon and Carbon/Metal Composite Materials Derived from Bio-Benzoxazine-Linked Precursor for CO_2 Capture and Energy Storage Applications, Int. J. Mol. Sci. 23 (2022) 347, https://doi.org/10.3390/ijms23010347.

[38] D. Kim, J. Kang, B. Yan, K.D. Seong, Y. Piao, Ambient Temperature Synthesis of Iron-Doped Porous Nickel PyrophosphateNanoparticles with Long-Term Chemical Stability for High-Performance Oxygen Evolution Reaction Catalysis and Supercapacitors, ACS Sustain. Chem. Eng. 8 (2020) 2843–2853, https://doi.org/10.1021/acssuschemeng.9b06920.

[39] X. Li, Z. Li, Y.W. Yang, Tetraphenylethylene-interweaving conjugated macrocycle polymer materials as two-photon fluorescence sensors for metal ions and organic molecules, Adv. Mater. 30 (2018) 1800177, https://doi.org/10.1002/adma.201800177.
[40] J.-S.M. Lee, A.I. Cooper, Advances in Conjugated Microporous Polymers, Chem. Rev. 20 (2020) 2171–2214, https://doi.org/10.1021/acs.chemrev.9b00399.
[41] M. Ejaz, M.G. Mohamed, W.C. Chang, S.W. Kuo, Synthesis and design of hypercrosslinked porous organic frameworks containing tetraphenylpyrazine unit for high-performance supercapacitor, J. Polym. Sci. (2023), https://doi.org/10.1002/pol.20230174.
[42] Z. Deng, H. Zhao, X. Cao, S. Xiong, G. Li, J. Deng, H. Yang, W. Zhang, Q. Liu, Enhancing Built-in Electric Field via Molecular Dipole Control in Conjugated Microporous Polymers for Boosting Charge Separation, ACS Appl. Mater. Interfaces 14 (2022) 35745–35754, https://doi.org/10.1021/acsami.2c08747.
[43] M. Ejaz, M.G. Mohamed, S.W. Kuo, Solid state chemical transformation provides a fully benzoxazine-linked porous organic polymer displaying enhanced CO_2 capture and supercapacitor performance, Polym. Chem. 14 (2023) 2494–2509, https://doi.org/10.1039/D3PY00158J.
[44] Y.S. Ye, M.G. Mohamed, W.C. Chen, S.W. Kuo, Integrating the multiple functionalities in metalloporphyrin porous organic polymers enabling strong polysulfide anchoring and rapid electrochemical kinetics in Li–S batteries, J. Mater. Chem. A 11 (2023) 9112–9124, https://doi.org/10.1039/D2TA09232H.
[45] S. Luo, Z. Zeng, H. Wang, W. Xiong, B. Song, C. Zhou, A. Duan, X. Tan, Q. He, G. Zeng, Z. Liu, R. Xiao, Recent progress in conjugated microporous polymers for clean energy: synthesis, modification, computer simulations, and applications, Prog. Polym. Sci. 115 (2021), 101374, https://doi.org/10.1016/j.progpolymsci.2021.101374.
[46] W. Zhang, H. Zuo, Z. Cheng, Y. Shi, Z. Guo, N. Meng, A. Thomas, Y. Liao, Macroscale conjugated microporous polymers: controlling versatile functionalities over several dimensions, Adv. Mater. 34 (2022) 2104952, https://doi.org/10.1002/adma.202104952.
[47] H. Wang, H. Wang, Z. Wang, L. Tang, G. Zeng, P. Xu, M. Chen, T. Xiong, C. Zhou, X. Li, D. Huang, Y. Zhu, Z. Wang, J. Tang, Covalent organic framework photocatalysts: structures and applications, Chem. Soc. Rev. 49 (2020) 4135–4165, https://doi.org/10.1039/D0CS00278J.
[48] D. Jiang, Covalent organic frameworks: an amazing chemistry platform for designing polymers, Chem 6 (2020) 2461–2483, https://doi.org/10.1016/j.chempr.2020.08.024.
[49] Z. Fu, J. Jia, J. Li, C. Liu, Transforming waste expanded polystyrene foam into hyper-crosslinked polymers for carbon dioxide capture and separation, Chem. Eng. J. 323 (2017) 557–564.
[50] M. Liu, L. Guo, S. Jin, B. Tan, Covalent triazine frameworks: synthesis and applications, J. Mater. Chem. A 7 (10) (2019) 5153–5172, https://doi.org/10.1016/j.cej.2017.04.090.
[51] J.M.H. Thomas, C. Mollart, L. Turner, P. Heasman, P. Fayon, A. Trewin, Artificial Synthesis of Conjugated Microporous Polymers via Sonogashira–Hagihara Coupling, J. Phys. Chem. B. 124 (2020) 7318–7326, https://doi.org/10.1021/acs.jpcb.0c04850.
[52] A. Yokoyama, H. Suzuki, Y. Kubota, K. Ohuchi, H. Higashimura, T. Yokozawa, Chain-growth polymerization for the synthesis of polyfluorene via Suzuki–Miyaura coupling reaction from an externally added initiator unit, J. Am. Chem. Soc. 129 (2007) 7236–7237, https://doi.org/10.1021/ja070313v.
[53] W. Huang, L. Su, Z. Bo, Hyperbranched Polymers with a Degree of Branching of 100% Prepared by Catalyst Transfer Suzuki– Miyaura Polycondensation, J. Am. Chem. Soc. 131 (2009) 10348–10349, https://doi.org/10.1021/ja9033846.
[54] M. Nojima, R. Saito, Y. Ohta, T. Yokozawa, Investigation of Mizoroki-Heck coupling polymerization as a catalyst-transfer condensation polymerization for synthesis of poly(p-phenylenevinylene), J. Polym. Sci., Part A: Polym. Chem. 53 (2015) 543–551, https://doi.org/10.1002/pola.27472.
[55] P. Wang, X. Miao, Y. Meng, Q. Wang, J. Wang, H. Duan, Y. Li, C. Li, J. Liu, L. Cao, Tetraphenylethene-Based Supramolecular Coordination Frameworks with Aggregation-Induced Emission for an Artificial Light-Harvesting System, ACS Appl. Mater. Interfaces 12 (2020) 22630–22639, https://doi.org/10.1021/acsami.0c04917.
[56] R. Arumugaperumal, M. Shellaiah, V. Srinivasadesikan, K. Awasthi, K.W. Sun, M. C. Lin, N. Ohta, W.S. Chung, Diversiform Nanostructures Constructed from Tetraphenylethene and Pyrene-Based Acid/Base Controllable Molecular Switching Amphiphilic [2]Rotaxanes with Tunable Aggregation-Induced Static Excimers, ACS Appl. Mater. Interfaces 12 (2020) 45222–45234, https://doi.org/10.1021/acsami.0c14107.
[57] M. Selvaraj, K. Rajalakshmi, D.H. Ahn, S.J. Yoon, Y.S. Nam, Y. Lee, Y. Xu, J. W. Song, K.B. Lee, Tetraphenylethene-based fluorescent probe with aggregation-induced emission behavior for Hg^{2+} detection and its application, Anal. Chim. Acta 1148 (2021), 238178, https://doi.org/10.1016/j.aca.2020.12.053.
[58] J. Bai, J. Peng, T. Xu, M. Bu, W. Chen, Y. Nie, J. Jia, A tetraphenylethene-based Schiff base AIEgen with a large Stokes shift as probe for highly sensitive and selective detection of aqueous Cu^{2+} ions and its application in cell imaging, Spectrochim. Acta A Mol. Biomol. Spectrosc. 290 (2023), 122190, https://doi.org/10.1016/j.saa.2022.122190.
[59] D. Pan, Y. Don, Y. Lu, G. Xiao, H. Chi, Z. Hu, AIE fluorescent probe based on tetraphenylethylene and morpholine-thiourea structures for detection of HClO, Anal. Chim. Acta 1235 (2022), 340559, https://doi.org/10.1016/j.aca.2022.340559.
[60] Y. Xiao, K. Zheng, N. Zhang, Y. Wang, J. Yan, D. Wang, X. Liu, Facile Synthesis of Tetraphenylethene (TPE)-Based Fluorophores Derived by π-Extended Systems: Opposite Mechanofluorochromism, Anti-Counterfeiting and Bioimaging, Eur. J. Chem. 29 (2023), e202203772, https://doi.org/10.1002/chem.202203772.
[61] A.O. Mousa, M.G. Mohamed, C.H. Chuang, S.W. Kuo, Carbonized Aminal-Linked Porous Organic Polymers Containing Pyrene and Triazine Units for Gas Uptake and Energy Storage, Polymers 15 1891 (2023), https://doi.org/10.3390/polym15081891.
[62] L. Mei, X. Cui, Q. Duan, Y. Li, X. Lv, H.G. Wang, Metal Phthalocyanine-Linked Conjugated Microporous Polymer Hybridized with Carbon Nanotubes as a High-Performance Flexible Electrode for Supercapacitors, Int. J. Hydrog. Energy 45 (2020) 22950–22958, https://doi.org/10.1016/j.ijhydene.2020.06.208.
[63] M.G. Mohamed, S.Y. Chang, M. Ejaz, M.M. Samy, A.O. Mousa, S.W. Kuo, Design and Synthesis of Bisulfone-Linked Two-Dimensional Conjugated Microporous Polymers for CO_2 Adsorption and Energy Storage, Molecules 28 (2023) 3234, https://doi.org/10.3390/molecules28073234.
[64] P.N. Singh, M.G. Mohamed, S.V. Chaganti, S.U. Sharma, M. Ejaz, J.T. Lee, S. W. Kuo, Rational Design of Ultrastable Conjugated Microporous Polymers Based on Pyrene and Perylene Units as High-Performance Organic Electrode Materials for Supercapacitor Applications, ACS Appl. Energy Mater. 6 (2023) 8277–8287, https://doi.org/10.1021/acsaem.3c01391.
[65] T.H. Weng, M.G. Mohamed, S.U. Sharma, I.M.A. Mekhemer, H.H. Chou, S.W. Kuo, Rationally Engineered Ultrastable Three-Dimensional (3D) Conjugated Microporous Polymers Containing Triptycene, Tetraphenylethene, and Benzothiadiazole Units as Exceptional High-Performance Organic Electrodes for Supercapacitors, ACS Appl. Energy Mater. 6 (2023) 9012–9024, https://doi.org/10.1021/acsaem.3c01933.
[66] M.G. Mohamed, A.M. Elewa, M.S. Li, S.W. Kuo, Construction and multifunctional of hypercrosslinked porous organic polymers containing ferrocene unit for high-performance iodine adsorption and supercapacitor, J. Taiwan Inst. Chem. Eng. 150 (2023), 105045, https://doi.org/10.1016/j.jtice.2023.105045.
[67] M.G. Mohamed, S.V. Chaganti, S.U. Sharma, M.M. Samy, M. Ejaz, J.T. Lee, K. Zhang, S.W. Kuo, Constructing Conjugated Microporous Polymers Containing the Pyrene-4,5,9,10-Tetraone Unit for Energy Storage, ACS Appl. Energy Mater. 5 (2022) 10130–10140, https://doi.org/10.1021/acsaem.2c01842.
[68] M.G. Mohamed, W.C. Chang, S.V. Chaganti, S.U. Sharma, J.T. Lee, S.W. Kuo, Dispersion of ultrastable crown-ether-functionalized triphenylamine and pyrene-linked porous organic conjugated polymers with single-walled carbon nanotubes as high-performance electrodes for supercapacitors, Polym. Chem. 14 (2023) 4589–4601, https://doi.org/10.1039/D3PY00708A.
[69] M.G. Mohamed, M.M. Samy, T.H. Mansoure, S.U. Sharma, M.S. Tsai, J.H. Chen, J. T. Lee, S.W. Kuo, Dispersions of 1,3,4-Oxadiazole-Linked Conjugated Microporous Polymers with Carbon Nanotubes as a High-Performance Electrode for Supercapacitors, ACS Appl. Energy Mater. 5 (2022) 3677–3688, https://doi.org/10.1021/acsaem.2c00100.
[70] M.M. Samy, M.G. Mohamed, S.W. Kuo, Pyrene-functionalized tetraphenylethylene polybenzoxazine for dispersing single-walled carbon nanotubes and energy storage, Compos. Sci. Technol. 199 (2020), 108360, https://doi.org/10.1016/j.compscitech.2020.108360.
[71] M. Madhu, W.L. Tseng, NaCl nanocrystal-encapsulated carbon dots as a solution-based sensor for phosphorescent sensing of trace amounts of water in organic solvents, Anal. Methods 13 (2021) 4949–4954, https://doi.org/10.1039/D1AY01202A.
[72] M. Madhu, C.M. Chao, C.Y. Ke, M.M. Hsieh, W.L. Tseng, Directed self-assembly of Ag^{+}-deposited MoS_2 quantum dots for colorimetric, fluorescent and fluorescence-lifetime sensing of alkaline phosphatase, Anal. Bioanal. Chem. 414 (2022) 1909–1919, https://doi.org/10.1007/s00216-021-03826-2.
[73] C.C. Ke, Y.C. Yang, W.L. Tseng, Synthesis of Blue-, Green-, Yellow-, and Red-Emitting Graphene-Quantum-Dot-Based Nanomaterials with Excitation-Independent Emission, Part. Part. Syst. Charact. 33 (2016) 132–139. Doi.org/10.1002/ppsc.201500196.
[74] H. Yang, Z. Ji, Y. Zeng, J. Zhang, L. Chen, H. Wang, Y. Yang, L. Guo, L. Li, Aggregation-induced emission monomer-based fluorescent molecularly imprinted poly(ionic liquid) synthesized by a one-pot method for sensitively detecting 4-nitrophenol, Anal. Methods 14 (2022) 1023–1030, https://doi.org/10.1039/D1AY02132J.
[75] M. Qayyum, T. Bushra, Z.A. Khan, H. Gul, S. Majeed, C. Yu, U. Farooq, A.J. Shaikh, S.A. Shahzad, Synthesis and Tetraphenylethylene-Based Aggregation-Induced Emission Probe for Rapid Detection of Nitroaromatic Compounds in Aqueous Media, ACS Omega 6 (2021) 25447–25460, https://doi.org/10.1021/acsomega.1c0343.